
On the Frequency-Bias of Coordinate-MLPs

Sameera Ramasinghe

Lachlan Macdonald

Simon Lucey

{firstname.lastname}@adelaide.edu.au
University of Adelaide

Abstract

We show that typical implicit regularization assumptions for deep neural networks (for regression) do not hold for coordinate-MLPs, a family of MLPs that are now ubiquitous in computer vision for representing high-frequency signals. Lack of such implicit bias disrupts smooth interpolations between training samples, and hampers generalizing across signal regions with different spectra. We investigate this behavior through a Fourier lens and uncover that as the bandwidth of a coordinate-MLP is enhanced, lower frequencies tend to get suppressed unless a suitable prior is provided explicitly. Based on these insights, we propose a simple regularization technique that can mitigate the above problem, which can be incorporated into existing networks without any architectural modifications.

1 Introduction

It is well-established that deep neural networks (DNN), despite mostly being used in the over-parameterized regime, exhibit remarkable generalization properties without explicit regularization [Neyshabur et al. \[2014\]](#), [Zhang et al. \[2017\]](#), [Savarese et al. \[2019\]](#), [Goodfellow et al. \[2016\]](#). This behavior questions the classical theories that predict an inverse relationship between model complexity and generalization, and is often referred to in the literature as the “implicit regularization” (or implicit bias) of DNNs [Li and Liang \[2018\]](#), [Kubo et al. \[2019\]](#), [Soudry et al. \[2018\]](#), [Poggio et al. \[2018\]](#). Characterizing this surprising phenomenon has been the goal of extensive research in recent years.

In contrast to this mainstream understanding, we show that coordinate-MLPs (or implicit neural networks), a class of MLPs that are specifically designed to overcome the *spectral bias* of regular MLPs, do not follow the same behavior. Spectral bias, as the name suggests, refers to the propensity of DNNs to learn functions with low frequencies, making them unsuited for encoding signals with high frequency content. Coordinate-MLPs, on the other hand, are architecturally modified MLPs (via specific activation functions [Sitzmann et al. \[2020\]](#), [Ramasinghe and Lucey \[2021\]](#) or positional embedding schemes [Mildenhall et al. \[2020\]](#), [Zheng et al. \[2021\]](#)) that can learn functions with high-frequency components. By virtue of this unique ability, coordinate-MLPs are now being used extensively in computer vision tasks for representing signals including texture generation [Henzler et al. \[2020\]](#), [Oechsle et al. \[2019\]](#), [Henzler et al. \[2020\]](#), [Xiang et al. \[2021\]](#), shape representation [Chen and Zhang \[2019\]](#), [Deng et al. \[2020\]](#), [Tiwari et al. \[2021\]](#), [Genova et al. \[2020\]](#), [Basher et al. \[2021\]](#), [Mu et al. \[2021\]](#), [Park et al. \[2019\]](#), and novel view synthesis [Mildenhall et al. \[2020\]](#), [Niemeyer et al. \[2020\]](#), [Saito et al. \[2019\]](#), [Sitzmann et al. \[2019\]](#), [Yu et al. \[2021\]](#), [Pumarola et al. \[2021\]](#), [Rebain et al. \[2021\]](#), [Martin-Brualla et al. \[2021\]](#), [Wang et al. \[2021\]](#), [Park et al. \[2021\]](#). However, as we will show in this paper, these architectural alterations entail an unanticipated drawback: coordinate-MLPs, trained by conventional means via stochastic gradient descent (SGD), are incapable of simultaneously generalizing well at both lower and higher ends of the spectrum, and thus, are not automatically biased towards less complex solutions (Fig. 1). Based on this observation, we question the popular understanding that the implicit bias of neural networks is more tied to SGD than the architecture [Zhang et al. \[2017, 2021\]](#).

Strictly speaking, the term “generalization” is not meaningful without context. For instance, consider a regression problem where the training points are sparsely sampled. Given more trainable parameters than the number of training points, a neural network can, in theory, learn infinitely many interpolants of the training points. Therefore, the challenge is to learn a function within a space restricted by certain priors and intuitions regarding the problem at hand. The generalization then can be measured by the extent to which the learned function is close to these prior assumptions about the task. Within a regression problem, one intuitive solution that is widely accepted by the practitioners (at least from an engineering perspective) is to have a form of “smooth” interpolation between the training points, where the low-order derivatives are bounded [Bishop \[2007\]](#). In classical machine learning, in order to restrict the class of learned functions, explicit regularization techniques were used [Craven and Wahba \[1978\]](#), [Wahba \[1975\]](#), [Kimeldorf and Wahba \[1970\]](#). Paradoxically, however, over-parameterized neural networks with extremely high capacity prefer to converge to such smooth solutions without any explicit regularization, despite having the ability to fit more complex functions [Zhang et al. \[2017, 2021\]](#).

Although this expectation of smooth interpolation is valid for both *a)* general regression problems with regular MLPs and *b)* high-frequency signal encoding with coordinate-MLPs, a key difference exists between their end-goals. In a general regression problem, we do not expect an MLP to perfectly fit the training data. Instead, we expect the MLP to learn a smooth curve that achieves a good trade-off between the bias and variance (generally tied to the anticipation of noisy data), which might not exactly overlap with the training points. In contrast, coordinate-MLPs are particularly expected to *perfectly fit* the training data that may include both low and high fluctuations, while interpolating smoothly between samples. This difficult task requires coordinate-MLPs to preserve a rich spectrum with both low and high frequencies (often with higher spectral energy for low frequencies, as the power spectrum of natural signals such as images tends to behave as $1/f^2$ [Ruderman \[1994\]](#)). We show that coordinate-MLPs naturally do *not* tend to converge to such solutions, despite the existence of possible solutions within the parameter space.

It should be pointed out that it *has* indeed been previously observed that coordinate-MLPs tend to produce noisy solutions when the bandwidth is increased excessively [Tancik et al. \[2020\]](#), [Ramasinghe and Lucey \[2021\]](#), [Sitzmann et al. \[2020\]](#). However, our work complements these previous observations: *First*, the existing works do not offer an explanation on why providing a coordinate-MLP with the capacity to add high frequencies to the spectrum would necessarily affect lower frequencies. In contrast, we elucidate this behavior through a Fourier lens, and show that as the spectrum of the coordinate-MLPs is enhanced via hyper-parameters or depth, the lower frequencies tend to be suppressed (for a given set of weights), hampering their ability to interpolate smoothly within low-frequency regions. *Second*, we interpret this behaviour from a model complexity angle, which allows us to incorporate network-depth into our analysis. *Third*, we show that this effect is common to many types of coordinate-MLPs, *i.e.*, MLPs with *a)* positional embeddings [Mildenhall et al. \[2020\]](#), *b)* periodic activations [Sitzmann et al. \[2020\]](#), and *c)* non-periodic activations [Ramasinghe and Lucey \[2021\]](#). Finally, we propose a simple regularization term that can enforce coordinate-MLPs to preserve both low and high frequencies in practice, enabling better generalization across the spectrum.

Our contributions are summarized below:

- We show that coordinate-MLPs are not implicitly biased towards low-complexity solutions, *i.e.*, typical implicit regularization assumptions do not hold for coordinate-MLPs. A bulk of previous mainstream works try to connect the implicit bias of neural networks to the properties of the optimization procedure (SGD), rather than the architecture [Zhang et al. \[2017, 2021\]](#). On the contrary, we provide counter-evidence that the implicit bias of neural networks might indeed be strongly tied to the architecture.
- We present a general result (Theorem 4.1), that can be used to obtain the Fourier transform of shallow networks with arbitrary activation functions and multi-dimensional inputs, even when the Fourier expressions are not directly integrable over the input space. Utilizing this result we derive explicit formulae to study shallow coordinate-MLPs from a Fourier perspective.
- Using the above expressions, we show that shallow coordinate-MLPs tend to suppress lower frequencies when the bandwidth is increased via hyper-parameters or depth, disrupting smooth interpolations. Further, we empirically demonstrate that these theoretical insights from shallow networks extrapolate well to deeper ones.

- We propose a simple regularization technique to enforce smooth interpolations between training samples while perfectly fitting the training points, preserving a rich spectrum. The proposed technique can be easily applied to existing coordinate-MLPs without any architectural modifications.

Our analysis stands out from previous theoretical research [Tancik et al. \[2020\]](#), [Ramasinghe and Lucey \[2021\]](#), [Zheng et al. \[2021\]](#) on coordinate-MLPs for several reasons: *a)* we work in a relatively realistic setting excluding assumptions such as infinite-width networks or linear models. Although we *do* consider shallow networks, we also take into account the effect of increasing depth. *b)* All our expressions are derived from first principles and do not demand the support of additional literature such as neural tangent kernel (NTK) theory. *c)* we analyze different types of coordinate-MLPs within a single framework where the gathered insights are common across each type.

2 Related works

Understanding and characterizing the astonishing implicit generalization properties of DNNs has been an important research topic in recent years. Despite the overwhelming empirical evidence, establishing a rigorous theoretical underpinning for this behavior has been a challenge to this date. The related research can be broadly categorized into two: investigating implicit regularization on the *a)* weight space [Bishop \[1995\]](#), [Soudry et al. \[2018\]](#), [Poggio et al. \[2018\]](#), [Gidel et al. \[2019\]](#) and the *b)* function space [Maennel et al. \[2018\]](#), [Kubo et al. \[2019\]](#), [Heiss et al. \[2019\]](#). Notably, [Maennel et al. \[2018\]](#) analyzed ReLU networks under macroscopic assumptions and affirmed that for given input data, there are only finitely many, “simple” functions that can be obtained using regular ReLU MLPs, independent of the network size. [Kubo et al. \[2019\]](#) showed that ReLU-MLPs interpolate between training samples almost linearly, and [Heiss et al. \[2019\]](#) took a step further, proving that the interpolations can converge to (nearly) spline approximations. Seminal works by [Zhang et al. \[2017\]](#) and [Zhang et al. \[2021\]](#) showed that these generalization properties are strongly connected to the SGD. In contrast, we show that coordinate-MLPs tend to converge to complex solutions (given enough capacity), despite being trained with SGD. Further, all above works consider shallow networks in order to obtain precise theoretical guarantees. Similarly, we also utilize shallow architectures for a part of our analysis. However, our work differs from some of the above-mentioned theoretical work, as we do not focus on establishing rigorous theoretical bounds on generalization. Rather, we uncover, to the best of our knowledge, a critically overlooked shortcoming of coordinate-MLPs, and present plausible reasoning for this phenomenon from a Fourier perspective. We give a brief exposition of coordinate-MLPs in the next section.

3 Coordinate-MLPs

Coordinate-MLPs aim to encode continuous signals $f : \mathbb{R}^n \rightarrow \mathbb{R}^m$, *e.g.*, images, sound waves, or videos, as their weights. The inputs to the network typically are low-dimensional coordinates, *e.g.*, (x, y) positions, and the outputs are the sampled signal values at each coordinate *e.g.*, pixel intensities. The key difference between coordinate-MLPs and regular MLPs is that the former is designed to encode signals with higher frequencies – mitigating the spectral bias of the latter – via specific architectural modifications. Below, we will succinctly discuss three types of coordinate-MLPs.

Random Fourier Feature (RFF) MLPs are compositions of a positional embedding layer and subsequent ReLU layers. Let Ω denote the probability space \mathbb{R}^n equipped with the Gaussian measure

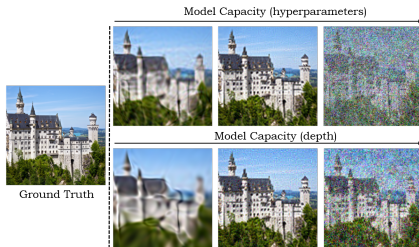


Figure 1: **Implicit regularization assumptions do not hold for Coordinate-MLPs.** The network is trained with 10% of the pixels in each instance. As the capacity of the network is increased via depth or hyperparameters, coordinate-MLPs tend to produce more complex solutions even though they are trained with SGD. This is in contrast to the regular-MLPs, where the networks converge to “smooth” solutions independent of the model capacity [Kubo et al. \[2019\]](#), [Heiss et al. \[2019\]](#). Further, this provides evidence that the implicit regularization of neural networks might be strongly linked to the architecture rather than the optimization procedure, as opposed to a mainstream understanding [Zhang et al. \[2017, 2021\]](#).

Further, this provides evidence that the implicit regularization of neural networks might be strongly linked to the architecture rather than the optimization procedure, as opposed to a mainstream understanding [Zhang et al. \[2017, 2021\]](#).

of standard deviation $2\pi\sigma > 0$. For $D \geq 1$, write elements \mathbf{L} of Ω^n as matrices $[\mathbf{l}_1, \dots, \mathbf{l}_D]$ composed of D vectors drawn independently from Ω . Then, the random Fourier feature (RFF) positional embedding $\gamma : \Omega^D \times \mathbb{R}^n \rightarrow \mathbb{R}^{2D}$ is

$$\gamma(\mathbf{L}, \mathbf{x}) := [\mathbf{e}(\mathbf{l}_1, \mathbf{x}), \dots, \mathbf{e}(\mathbf{l}_D, \mathbf{x})]^T, \quad (1)$$

where $\mathbf{e} : \Omega \times \mathbb{R}^n \rightarrow \mathbb{R}^2$ is the random function defined by the formula

$$\mathbf{e}(\mathbf{l}, \mathbf{x}) := [\sin(\mathbf{l} \cdot \mathbf{x}), \cos(\mathbf{l} \cdot \mathbf{x})]. \quad (2)$$

The above layer is then followed by a stack of ReLU layers.

Sinusoidal MLPs were originally proposed by [Sitzmann et al. \[2020\]](#). Let \mathbf{W} and \mathbf{b} be the weights and the bias of a hidden layer of a sinusoidal coordinate-MLP, respectively. Then, the output of the hidden-layer is $\sin(2\pi a(\mathbf{W} \cdot \mathbf{x} + \mathbf{b}))$, where a is a hyper-parameter that can control the spectral-bias of the network and \mathbf{x} is the input.

Gaussian MLPs are a recently proposed type of coordinate-MLP by [Ramasinghe and Lucey \[2021\]](#).

The output of a Gaussian hidden-layer is defined by $e^{-\left(\frac{\mathbf{w} \cdot \mathbf{x} + \mathbf{b}}{2\sigma^2}\right)^2}$, where σ is a hyper-parameter.

In the next section, we will derive a general result that can be used to obtain the Fourier transform of an arbitrary multi-dimensional shallow MLP (given that the 1D Fourier transform of the activation function exists), which is used as the bedrock in a bulk of our derivations later.

4 Fourier transform of a shallow MLP

Let $\mathcal{G} : \mathbb{R}^n \rightarrow \mathbb{R}$ be an MLP with a single hidden layer with m neurons, and a point-wise activation function $\alpha : \mathbb{R} \rightarrow \mathbb{R}$. Suppose we are interested in obtaining the Fourier transform $\hat{\mathcal{G}}$ of \mathcal{G} . Since the bias only contributes to the DC component, we formulate \mathcal{G} as $\mathcal{G} = \sum_{i=1}^m w_i^{(2)} \alpha(\mathbf{w}_i^{(1)} \cdot \mathbf{x})$, where $\mathbf{w}_i^{(1)}$ are rows of the first-layer affine weight matrix, input to the i^{th} hidden neuron is $\mathbf{w}_i^{(1)} \cdot \mathbf{x}$, and $w_i^{(2)}$ are the weights of the last layer. Since the Fourier transform is a linear operation, it is straightforward to see that

$$\hat{\mathcal{G}} = \sum_{i=1}^m w_i^{(2)} \hat{\alpha}(\mathbf{w}_i^{(1)} \cdot \mathbf{x}). \quad (3)$$

Thus, by obtaining the Fourier transform of $f(\mathbf{x}) := \alpha(\mathbf{w} \cdot \mathbf{x})$, it is possible to derive the Fourier transform of the MLP. However, doing so using the standard definition of the multi-dimensional Fourier transform can be infeasible in some cases. For example, consider a Gaussian-MLP. Then, one can hope to calculate the Fourier transform of $f(\mathbf{x})$ as $\hat{f}(\mathbf{k}) = \int_{\mathbb{R}^n} e^{-\left(\frac{\mathbf{w} \cdot \mathbf{x}}{2\sigma^2} + 2\pi i \mathbf{x} \cdot \mathbf{k}\right)} d\mathbf{x}$. However, note that there exists an $n - 1$ dimensional subspace where $(\mathbf{w} \cdot \mathbf{x})$ is zero and thus, the first term inside the exponential becomes 0 in these cases. Therefore the Fourier transform does not exist as a function. Nonetheless, f defines a tempered distribution, and its Fourier transform \hat{f} can therefore be calculated by fixing a Schwartz test function φ on \mathbb{R}^n and using the identity $\langle \hat{f}, \varphi \rangle = \langle f, \hat{\varphi} \rangle$, defining the Fourier transform of the tempered distribution f . Here $\langle \cdot, \cdot \rangle$ denotes the pairing between distributions and test functions (see Chapter 8 of [Friedlander and Joshi \[1999\]](#) for this background). Formally, we present the following theorem, whose proof we defer to the appendix.

Theorem 4.1. *The Fourier transform of $f(\mathbf{x}) := \alpha(\mathbf{w} \cdot \mathbf{x})$ where $\mathbf{w}, \mathbf{x} \in \mathbb{R}^n$ is the distribution*

$$\hat{f}(\mathbf{k}) = \frac{(2\pi)^{\frac{n}{2}}}{|\mathbf{w}|} \hat{\alpha}\left(\frac{\mathbf{w}}{|\mathbf{w}|^2} \cdot \mathbf{k}\right) \delta_{\mathbf{w}}(\mathbf{k}),$$

where $\delta_{\mathbf{w}}(\mathbf{k})$ is the Dirac delta distribution which concentrates along the line spanned by \mathbf{w} . \square

Next, using the above result, we will gather useful insights into different types of coordinate-MLPs from a Fourier perspective.

5 Effect of hyperparameters

In this section, we will primarily explore the effect of hyperparameters on the spectrum of coordinate-MLPs, among other key insights.

5.1 Gaussian-MLP

The Fourier transform of the Gaussian activation is $\hat{\alpha}(k) = \sqrt{2\pi}\sigma e^{-(\sqrt{2\pi}k\sigma)^2}$. Now, using Theorem 4.1, we can obtain the Fourier transform of a Gaussian-MLP with a single hidden layer as

$$\sum_{i=1}^m w_i^{(2)} \frac{(2\pi)^{\frac{n+1}{2}} \sigma}{|\mathbf{w}_i^{(1)}|} e^{-\left(\sqrt{2\pi} \frac{\mathbf{w}_i^{(1)}}{|\mathbf{w}_i^{(1)}|^2} \cdot \mathbf{k}\sigma\right)^2} \delta_{\mathbf{w}_i^{(1)}}(\mathbf{k}). \quad (4)$$

Discussion: For fixed $\mathbf{w}_i^{(1)}$'s and σ , the spectral energy is decayed as \mathbf{k} is increased. A practitioner can increase the energy of higher frequencies by decreasing σ . Second, although decreasing σ can increase the energy of higher frequencies (for given weights), it simultaneously suppresses the energies of lower frequencies due to the σ term outside the exponential. Third, one can achieve the best of both worlds (*i.e.*, incorporate higher-frequencies to the spectrum while maintaining higher energies for lower-frequencies) by appropriately tuning $\mathbf{w}_i^{(1)}$'s. To make the above theoretical observations clearer, we demonstrate a toy example in Fig. 2.

5.2 Sinusoidal-MLPs

Similar to the Gaussian-MLP, the Fourier transform of a sinusoidal-MLP with a single hidden-layer can be obtained as

$$\sum_{i=1}^m w_i^{(2)} \frac{(2\pi)^{\frac{n}{2}}}{2|\mathbf{w}_i^{(1)}|} \delta_{\mathbf{w}_i^{(1)}}(\mathbf{k}) \left(\delta\left(\frac{\mathbf{w}_i^{(1)}}{|\mathbf{w}_i^{(1)}|^2} \cdot \mathbf{k} - a\right) + \delta\left(\frac{\mathbf{w}_i^{(1)}}{|\mathbf{w}_i^{(1)}|^2} \cdot \mathbf{k} + a\right) \right), \quad (5)$$

Discussion: According to Eq. 5, the only frequencies present in the spectrum are multiples $\mathbf{k} = a\mathbf{w}_i^{(1)}$ of the weight vectors $\mathbf{w}_i^{(1)}$. It follows that the magnitudes of the frequencies present in the spectrum are lower-bounded by the number $a \min\{|\mathbf{w}_i|\}$. Thus for a given set of weights, one can add higher frequencies to the spectrum by increasing a . At the same time, the spectrum can be *balanced* by minimizing some \mathbf{w}_i 's accordingly.

5.3 RFF-MLPs

We consider a shallow RFF-MLP $\mathbb{R}^n \rightarrow \mathbb{R}$ with a single hidden ReLU layer. Recall that the positional embedding scheme is defined following Eq. 1 and 2. The positional embedding layer γ is then followed by a linear transformation $A : \mathbb{R}^{2D} \rightarrow \mathbb{R}^{2D}$ yielding

$$f_2(\mathbf{L}, \mathbf{x})^i = \sum_j a_j^i \gamma(\mathbf{L}, \mathbf{x})^j,$$

which is then followed by ReLU activations and an affine transformation. ReLU activations can be approximated via linear combinations of various polynomial basis functions Ali et al. [2020], Telgarsky [2017]. One such set of polynomials is Newman polynomials defined as

$$N_m(x) := \prod_{i=1}^{m-1} (x + \exp(-i/\sqrt{n})).$$

It is important to note that although we stick to the Newman polynomials in the subsequent derivations, the obtained insights are valid for *any* polynomial approximation, as they only depend on the power terms of the polynomial approximation. Moving on, for $m \geq 5$, we show in the appendix that the spectrum of the RFF-MLP is concentrated on frequencies

$$\mathbf{k} = \sum_{j=1}^D ((2a_{2j-1} - k_{2j-1}) + (2a_{2j} - k_{2j})) \mathbf{l}_j, \quad (6)$$

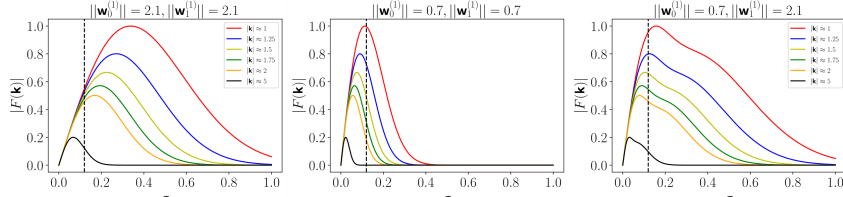


Figure 2: **Toy example (a Gaussian-MLP $\mathbb{R}^2 \rightarrow \mathbb{R}$ with a single hidden layer consisting of two neurons):** The behavior of the spectrum against σ and the weights of the network is shown. $\mathbf{w}_0^{(1)}$ and $\mathbf{w}_1^{(1)}$ are the first and second rows of the first-layer affine weight matrix. *Left:* By decreasing σ , the network can include higher frequencies to the spectrum. However, as the high-frequency components are added to the spectrum, the relative energies of the low-frequency components decrease. *Middle:* The network can still gain high energies for lower frequencies at lower σ by decreasing $|\mathbf{w}_0^{(1)}|$ and $|\mathbf{w}_1^{(1)}|$. However, in this case, the high-frequency components are removed from the spectrum. *Right:* By appropriately tuning $|\mathbf{w}_0^{(1)}|$ and $|\mathbf{w}_1^{(1)}|$, the spectrum can include higher-frequency components while preserving the low-frequency energies. All the intensities are normalized for better comprehension.

for non-negative integers k_1, \dots, k_{2D} adding to $m - 2$, and for all non-negative integers $a_j \leq k_j$ for all $j = 1, \dots, 2D$. Here we recall that D is the dimension determined by the choice of RFF positional embedding.

Discussion: Recall that if $U, V \sim \mathcal{N}(0, \sigma^2)$, then, $\text{Var}(t_1 U + t_2 V) = (t_1^2 + t_2^2) \sigma^2$. Therefore the overall spectrum can be made wider by increasing the standard deviation σ of the distribution from which the \mathbf{l}_j are drawn. However, since the D is constant, a larger σ makes frequencies less concentrated in the lower end, reducing the overall energy of the low frequency components. Nonetheless, the spectrum can be altered via adjusting the network weights.

Thus far, we established that in all three types of coordinate-MLPs, a rich spectrum consisting of both low and high frequencies can be preserved by properly tuning the weights and hyperparameters. However, coordinate-MLPs tend to suppress lower frequencies when trained without explicit regularization (see Fig. 5). Moreover, note that in each Fourier expression, the Fourier components cease to exist if \mathbf{k} is not in the direction of $\mathbf{w}_i^{(1)}$, due to the Dirac-delta term. Therefore, the angles between $\mathbf{w}_i^{(1)}$'s should be increased, in order to add frequency components in different directions.

6 Effect of depth

This section investigates the effects of increasing depth on the spectrum of coordinate-MLPs. Comprehensive derivations of the expressions in this section can be found in the Appendix. Let a stack of layers be denoted as $\kappa : \mathbb{R}^n \rightarrow \mathbb{R}^d$. Suppose we add another stack of layers $\eta : \mathbb{R}^d \rightarrow \mathbb{R}$ on top of $\kappa(\cdot)$ to construct the MLP $\eta \circ \kappa : \mathbb{R}^n \rightarrow \mathbb{R}$. The Fourier transform of the composite function then becomes,

$$\widehat{(\eta \circ \kappa)}(\mathbf{k}) = \left(\frac{1}{\sqrt{2\pi}} \right)^n \langle \hat{\eta}(\cdot), \beta(\mathbf{k}, \cdot) \rangle, \quad (7)$$

where, $\beta(\mathbf{k}, \mathbf{t}) = \int_{\mathbb{R}^n} e^{i(\mathbf{t} \cdot \kappa(\mathbf{x}) - \mathbf{k} \cdot \mathbf{x})}$. That is, the composite Fourier transform is the projection of $\hat{\eta}$ on to $\beta(\cdot)$. The maximum magnitude frequency $\mathbf{k}_{\eta \circ \kappa}^*$ present in the spectrum of $\widehat{(\eta \circ \kappa)}$ is

$$\mathbf{k}_{\eta \circ \kappa}^* = \max_{|\mathbf{u}|=1} (\mathbf{k}_{\hat{\eta}, \mathbf{u}}^* \max_{\mathbf{x}} (\mathbf{u} \cdot \kappa'(\mathbf{x}))), \quad (8)$$

where $\mathbf{k}_{\hat{\eta}, \mathbf{u}}$ is the maximum frequency of $\hat{\eta}$ along \mathbf{u} Bergner et al. [2006]. Thus, the addition of a set of layers η with sufficiently rich spectrum tends to increase the maximum magnitude frequency expressible by the network. Next, we focus on the impact on lower frequencies by such stacking. It is important to note that the remainder of the discussion in this section is not a rigorous theoretical derivation, but rather, an intuitive explanation.

We consider the 1D case for simplicity. Our intention is to explore the effect of adding more layers on $\langle \hat{\eta}(\cdot), \beta(\mathbf{k}, \cdot) \rangle$. Note that β is an integral of an oscillating function with unit magnitude. The integral of an oscillating function is non-negligible only at points where the phase is close to zero, *i.e.*, points of stationary phase. It can be deduced that at such points the following condition needs to be satisfied,

$$\min(\kappa'(x)) < \frac{k}{t} < \max(\kappa'(x)). \quad (9)$$

From the previous analysis, we established that progressively adding layers increases the maximum frequency of the composite function. This causes κ to have rapid fluctuations, encouraging $\min(\kappa'(x))$ to increase as the network gets deeper (note that the definition of κ keeps changing as more layers are added). Note that as $\min(\kappa')$ is increased, for smaller k 's, Eq. 9 is not satisfied. On the other hand, β is non-negligible only at points where Eq. 9 is satisfied. Thus, according to Eq. 9, smaller k 's causes the quantity $\langle \hat{\eta}(\cdot), \beta(\mathbf{k}, \cdot) \rangle$ to be smaller, which encourages suppressing the energy of the lower frequencies of $(\eta \circ \kappa)$. Rigorously speaking, increasing the bandwidth of the network by adding more layers does not necessarily have to increase $\min(\kappa'(x))$. However, our experimental results strongly suggest that this is the case. Summarizing our insights from Sec. 4, 5 and Sec. 6, we state the following remarks.

Remark 6.1. *In order to gain a richer spectrum, the columns of the affine weight matrices of the coordinate-MLPs need to point in different directions. Ideally, the column vectors should lie along the frequency directions in the target signal.*

Remark 6.2. *The spectrum of the coordinate-MLPs can be altered either by tuning the hyperparameters or changing the depth. In practice, when higher frequencies are added to the spectrum, the energy of lower frequencies tend to be suppressed, disrupting smooth interpolations between samples. However, better solutions exist in the parameter space, thus, an explicit prior is needed to bias the network weights towards those solutions.*

In the next section, we will focus on proposing a regularization mechanism that can aid the coordinate-MLPs in finding a solution with a better spectrum.

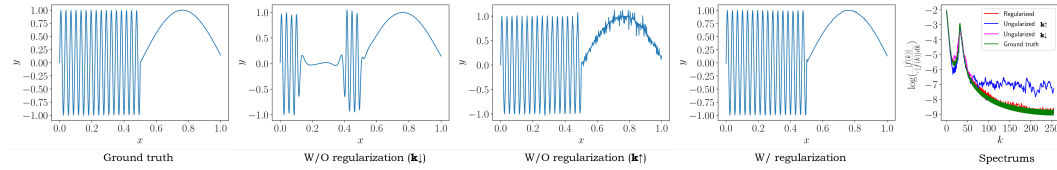


Figure 3: The effect of explicit regularization. When trained under conventional means, coordinate MLPs cannot generalize well at both higher and lower ends of the spectrum. This hinders the generalization performance of coordinate-MLPs when the target signal comprises regions with different spectral properties. When the network has insufficient bandwidth, the network cannot correctly capture high-frequency modes. When the network is tuned to have a higher bandwidth, the network fails at modeling lower frequencies. In contrast, the network can preserve a better spectrum with the proposed regularization scheme. This example uses a 4-layer sinusoid-MLP trained with 33% of the total samples.

7 Regularizing coordinate-MLPs

The spectrum of a function is inherently related to the magnitude of its derivatives. For instance, consider a function $f : \mathbb{R} \rightarrow \mathbb{R}$ defined on a finite interval ϵ . Then, it can be shown that $\max_{x \in \epsilon} \left| \frac{df(x)}{dx} \right| \leq 2\pi \int_{-\infty}^{\infty} |k \hat{f}(k)| dk$ (see Appendix). For multi-dimensions, we can encourage the spectrum to have a higher or lower frequency support by appropriately constraining the fluctuations along the corresponding directions. We shall now discuss how this fact may be utilized in regularizing coordinate-MLPs.

Let us consider a coordinate-MLP $f : \mathbb{R}^n \rightarrow \mathbb{R}$, which we factorise as $f = \tilde{f} \circ g$, where \tilde{f} is the final layer. Then by the chain rule:

$$\left| \frac{df}{dx} \right| = \sqrt{\left[\frac{\partial \tilde{f}}{\partial \mathbf{y}} \cdot \frac{\partial g}{\partial \mathbf{x}} \right] \left[\frac{\partial \tilde{f}}{\partial \mathbf{y}} \cdot \frac{\partial g}{\partial \mathbf{x}} \right]^T} = \sqrt{\frac{\partial \tilde{f}}{\partial \mathbf{y}} \cdot \mathbf{J} \mathbf{J}^T \cdot \left[\frac{\partial \tilde{f}}{\partial \mathbf{y}} \right]^T}, \quad (10)$$

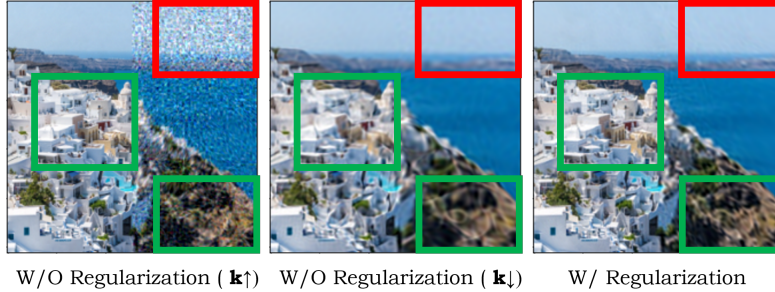


Figure 4: **Qualitative results for encoding signals with uneven sampling (zoom in for a better view).** A Gaussian-MLP is trained to encode an image, where the left half of the image is sampled densely, and the right half is sampled with 10% pixels. The reconstruction results are shown. When the bandwidth of the Gaussian-MLP is adjusted to match the sampling procedure of a particular half, the other half demonstrates poor reconstruction. In contrast, when regularized, coordinate-MLPs can preserve both low and high frequencies, giving a balanced reconstruction. Contrast the green and red areas across each setting.

where \mathbf{J} is the Jacobian of g . Let $\mathbf{A} = \mathbf{J}\mathbf{J}^T$. In order to minimize $|\frac{df}{d\mathbf{x}}|$, it suffices to minimize the magnitude of the components of \mathbf{J} , which is equivalent to minimizing the trace of \mathbf{A} . Recall that $\text{tr}(\mathbf{A}) = \sum_k \lambda_k$, where λ_k are the eigenvalues of \mathbf{A} . One has $\lim_{|\epsilon| \rightarrow 0} \frac{|g(\mathbf{x}) - g(\mathbf{x} + \epsilon u_k)|}{|\epsilon u_k|} = \sqrt{\lambda_k}$, where u_k are the eigenvectors of \mathbf{A} . Therefore, minimizing an eigenvalue of \mathbf{A} is equivalent to restricting the fluctuations of g along the direction of its associated eigenvector. By this logic, the ideal regularization procedure would be to identify the directions in the spectrum of the target signal where the frequency support is low, and restrict λ_k 's corresponding to those directions. According to our derivations in the previous sections, this would only be possible by regularizing \mathbf{w}_i 's, since in practice, we use hyperparameters for coordinate-MLPs that allow higher bandwidth. However, this is a cumbersome task and we empirically found that there is a much simpler approximation for this procedure that can give equivalent results (see Appendix) as,

$$\mathcal{L}_r = \frac{|g(\bar{\mathbf{x}}) - g(\bar{\mathbf{x}} + \xi)|}{|\xi|}, \quad (11)$$

where $\bar{\mathbf{x}}$ are randomly sampled from the coordinate space and $\xi \sim \mathcal{N}(0, \Sigma)$ where Σ is diagonal with small values. The total loss function for the coordinate-MLP then becomes $\mathcal{L}_{total} = \mathcal{L}_{MSE} + \epsilon \mathcal{L}_r$ where ϵ is a small scalar coefficient and \mathcal{L}_{MSE} is the usual mean squared error loss. The total loss can also be interpreted as encouraging the networks to obtain the smoothest possible solution while perfectly fitting the training samples. By the same argument, one can apply the above regularization on an arbitrary layer, including the output, although we empirically observed that the penultimate layer performs best. Although the proposed loss has a similar goal to the popular *total-variation loss*, the former converges to more desired solutions (see Appendix).

8 Experiments

In this section, we will show that the insights developed thus far extend well to deep networks in practice.

8.1 Encoding signals with uneven sampling

The earlier sections showed that coordinate-MLPs tend to suppress low frequencies when the network attempts to add higher frequencies to the spectrum. This can lead to poor performance when the target signal is unevenly sampled because, if the sampling is dense, the network needs to incorporate higher frequencies to properly encode the signal. Thus, at regions where the sampling is sparse, the network fails to produce smooth interpolations, resulting in noisy reconstructions. On the other hand, if the bandwidth of the network is restricted via hyperparameters or depth, the network can smoothly interpolate in sparse regions, but fails to encode information with high fidelity at dense regions. Explicit regularization can aid the network in finding a properly balanced spectrum in the solution space. Fig. 3 shows an example for encoding a 1D signal. Fig. 4 illustrates a qualitative example in encoding a 2D image. Table 1 depicts quantitative results on the natural dataset by [Tancik](#)

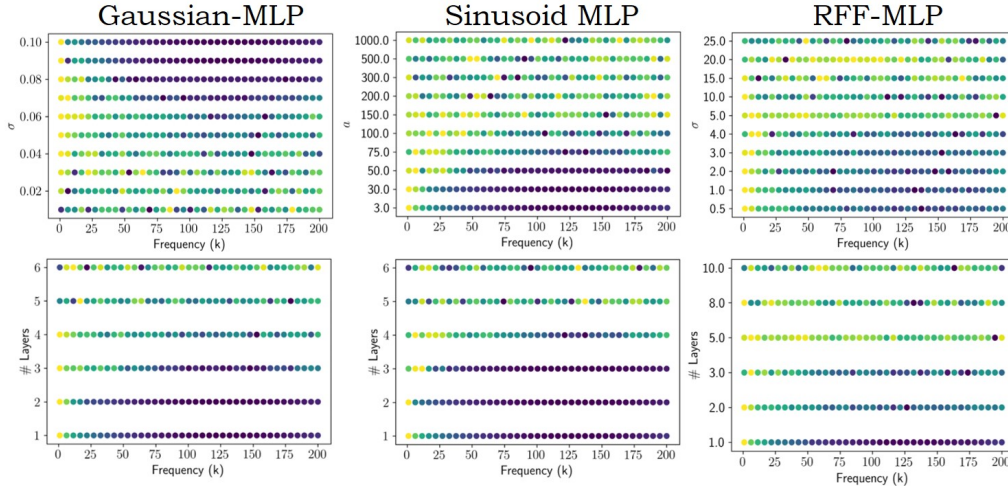


Figure 5: **Spectra of the coordinate-MLPs against hyperparameters and depth.** We train each network instance to encode a sound wave with 33% sampling. The heat indicates the intensity of the corresponding frequency component after trained with the MSE loss. As illustrated, when the capacity of the network is increased via hyperparameters or depth, the networks tend to converge to solutions with suppressed low-frequency components.

W/O Regularization ($k \downarrow$)			
Type	L-PSNR	R-PSNR	T-PSNR
Gaussian-MLP	30.12	22.47	27.72
Sinusoid-MLP	30.49	21.93	26.89
RFF-MLP	29.89	22.33	26.44
W/O Regularization ($k \uparrow$)			
Type	L-PSNR	R-PSNR	T-PSNR
Gaussian-MLP	33.43	18.14	22.80
Sinusoid-MLP	32.17	19.30	23.49
RFF-MLP	32.24	19.11	22.19
Regularized			
Type	L-PSNR	R-PSNR	T-PSNR
Gaussian-MLP	33.11	23.31	30.15
Sinusoid-MLP	31.59	22.66	29.94
RFF-MLP	31.99	22.91	29.59

Table 1: **Encoding images with uneven sampling.** In each training instance, the left half of the image is sampled densely, and the right half is sampled with 10% pixels. With unregularized coordinate-MLPs, when the hyperparameters are tuned to match the sampling of a particular half, the reconstruction of the other half is poor. In contrast, the encoding performance is balanced when regularized. We use 4-layer networks for this experiment.

et al. [2020]. L-PSNR, R-PSNR, and T-PSNR means PSNR evaluated on the left, right and the total image, respectively.

8.2 Encoding signals with different local spectral properties

The difficulty in generalizing well across different regions in the spectrum hinders encoding natural signals such as images when the sampling is sparse, as they tend to contain both “flat” and “fluctuating” regions, and the network has no prior on how to interpolate in these different regions. See Fig. 6 and Table 2 for qualitative and quantitative results. As evident, the coordinate-MLP struggles to smoothly interpolate between samples under a single hyperparameter setting. We also assess the performance of the regularization on NeRF style data. The results are depicted in Fig. 7 and Table. 3.

8.3 Effect of increasing capacity

Our derivations in Sec. 4 and 6 showed that shallow coordinate-MLPs tend to suppress lower frequencies when the capacity of the network is increased via depth or hyperparameters. Our empirical results show that this is indeed the case for deeper networks as well (see Fig. 5).

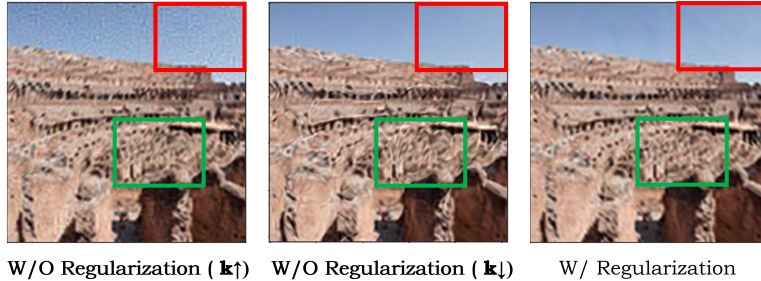


Figure 6: A single hyperparameter setting cannot generalize well across the spectrum unless regularized (better viewed in zoom). With sparse sampling (10% of the total pixels), coordinate-MLPs exhibit inferior reconstruction performance across regions with different spectra. In comparison, regularized networks can achieve the best of both worlds. Compare the highlighted areas across each setting.

STL		
Type	W/O Regularization	Regularized
Gaussian-MLP	22.11	24.17
Sinusoid-MLP	21.97	25.01
RFF-MLP	22.03	23.31
ImageNet		
Gaussian-MLP	24.59	26.77
Sinusoid-MLP	23.81	26.90
RFF-MLP	23.11	25.94

Table 2: **Encoding images with sparse sampling.** We compare the performance over the STL dataset Coates et al. [2011] and a sub-sampled version of ImageNet with 10% sampling. Regularized coordinate-MLPs show superior performance due to better interpolation properties. We use 4-layer coordinate-MLPs for this experiment.

Loss	PSNR	SSIM
MSE + L1	30.91	0.947
MSE + L2	30.14	0.935
MSE	30.87	0.940
MSE+TV loss	29.11	0.909
MSE+proposed reg.	32.01	0.951

Table 3: **Quantitative comparison in novel view synthesis on the real synthetic dataset [Mildenhall et al., 2020].** The proposed regularization achieves better results. In contrast, TV loss worsens the performance. Note that we use TV loss with 0.001 weight, and its performance converges to vanilla MSE loss as the weight gets smaller. L1 regularization improves the results slightly, but still is inferior to the proposed regularizer.

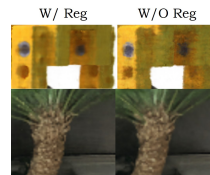


Figure 7: **Our regularization is able to achieve better reconstructions (NeRF data).** Top row: Proposed regularization suppresses the unnecessary higher frequencies. Bottom row: we can obtain sharper results by increasing the frequency support of the positional embedding layer and then applying the regularization. Cropped and zoomed in for better viewing.

9 Limitations

Currently, our work theoretically analyzes coordinate-networks within a constrained shallow setting. Although the insights we gather from this restricted setting can be empirically extrapolated to deeper networks (as we have shown), future research should focus on deriving rigorous formulae to analyze practical, deeper coordinate networks. Further, the current approach involves manually tuning the weights of the loss components, which requires a fair amount of domain knowledge. Perhaps, a more in-depth study can reveal general guidelines for tuning these parameters.

10 Conclusion

We show that the traditional implicit regularization assumptions do not hold in the context of coordinate-MLPs. We focus on establishing plausible reasoning for this phenomenon from a Fourier angle and discover that coordinate-MLPs tend to suppress lower frequencies when the capacity is increased unless explicitly regularized. We further show that the developed insights are valid in practice.

References

- Ramy E Ali, Jinhyun So, and A Salman Avestimehr. On polynomial approximations for privacy-preserving and verifiable relu networks. *arXiv preprint arXiv:2011.05530*, 2020.
- Abol Basher, Muhammad Sarmad, and Jani Boutellier. Lightsal: Lightweight sign agnostic learning for implicit surface representation. *arXiv preprint arXiv:2103.14273*, 2021.
- Steven Bergner, Torsten Moller, Daniel Weiskopf, and David J Muraki. A spectral analysis of function composition and its implications for sampling in direct volume visualization. *IEEE transactions on visualization and computer graphics*, 12(5):1353–1360, 2006.
- Christopher M Bishop. Regularization and complexity control in feed-forward networks. 1995.
- Christopher M Bishop. Pattern recognition and machine learning (information science and statistics), 2007.
- Blake Bordelon, Abdulkadir Canatar, and Cengiz Pehlevan. Spectrum dependent learning curves in kernel regression and wide neural networks. In *International Conference on Machine Learning*, pages 1024–1034. PMLR, 2020.
- Yuan Cao, Zhiying Fang, Yue Wu, Ding-Xuan Zhou, and Quanquan Gu. Towards understanding the spectral bias of deep learning. *arXiv preprint arXiv:1912.01198*, 2019.
- Zhiqin Chen and Hao Zhang. Learning implicit fields for generative shape modeling. In *Proceedings of the IEEE/CVF Conference on Computer Vision and Pattern Recognition*, pages 5939–5948, 2019.
- Adam Coates, Andrew Ng, and Honglak Lee. An analysis of single-layer networks in unsupervised feature learning. In *Proceedings of the fourteenth international conference on artificial intelligence and statistics*, pages 215–223. JMLR Workshop and Conference Proceedings, 2011.
- Peter Craven and Grace Wahba. Smoothing noisy data with spline functions. *Numerische mathematik*, 31(4):377–403, 1978.
- Boyang Deng, John P Lewis, Timothy Jeruzalski, Gerard Pons-Moll, Geoffrey Hinton, Mohammad Norouzi, and Andrea Tagliasacchi. Nasa neural articulated shape approximation. In *Computer Vision—ECCV 2020: 16th European Conference, Glasgow, UK, August 23–28, 2020, Proceedings, Part VII 16*, pages 612–628. Springer, 2020.
- F. G. Friedlander and M. Joshi. *Introduction to the Theory of Distributions*. Cambridge University Press, 1999.
- Kyle Genova, Forrester Cole, Avneesh Sud, Aaron Sarna, and Thomas Funkhouser. Local deep implicit functions for 3d shape. In *Proceedings of the IEEE/CVF Conference on Computer Vision and Pattern Recognition*, pages 4857–4866, 2020.
- Gauthier Gidel, Francis Bach, and Simon Lacoste-Julien. Implicit regularization of discrete gradient dynamics in linear neural networks. *arXiv preprint arXiv:1904.13262*, 2019.
- Ian Goodfellow, Yoshua Bengio, and Aaron Courville. *Deep learning*. MIT press, 2016.
- Jakob Heiss, Josef Teichmann, and Hanna Wutte. How implicit regularization of neural networks affects the learned function—part i. *arXiv*, pages 1911–02903, 2019.
- Philipp Henzler, Niloy J Mitra, and Tobias Ritschel. Learning a neural 3d texture space from 2d exemplars. In *Proceedings of the IEEE/CVF Conference on Computer Vision and Pattern Recognition*, pages 8356–8364, 2020.
- George S Kimeldorf and Grace Wahba. A correspondence between bayesian estimation on stochastic processes and smoothing by splines. *The Annals of Mathematical Statistics*, 41(2):495–502, 1970.
- Masayoshi Kubo, Ryotaro Banno, Hidetaka Manabe, and Masataka Minoji. Implicit regularization in over-parameterized neural networks. *arXiv preprint arXiv:1903.01997*, 2019.

- Yuanzhi Li and Yingyu Liang. Learning overparameterized neural networks via stochastic gradient descent on structured data. *arXiv preprint arXiv:1808.01204*, 2018.
- Tao Luo, Zheng Ma, Zhi-Qin John Xu, and Yaoyu Zhang. Theory of the frequency principle for general deep neural networks. *arXiv preprint arXiv:1906.09235*, 2019.
- Tao Luo, Zheng Ma, Zhi-Qin John Xu, and Yaoyu Zhang. On the exact computation of linear frequency principle dynamics and its generalization. *arXiv preprint arXiv:2010.08153*, 2020.
- Hartmut Maennel, Olivier Bousquet, and Sylvain Gelly. Gradient descent quantizes relu network features. *arXiv preprint arXiv:1803.08367*, 2018.
- Ricardo Martin-Brualla, Noha Radwan, Mehdi SM Sajjadi, Jonathan T Barron, Alexey Dosovitskiy, and Daniel Duckworth. Nerf in the wild: Neural radiance fields for unconstrained photo collections. In *Proceedings of the IEEE/CVF Conference on Computer Vision and Pattern Recognition*, pages 7210–7219, 2021.
- Ben Mildenhall, Pratul P Srinivasan, Matthew Tancik, Jonathan T Barron, Ravi Ramamoorthi, and Ren Ng. Nerf: Representing scenes as neural radiance fields for view synthesis. In *European Conference on Computer Vision*, pages 405–421. Springer, 2020.
- Jiteng Mu, Weichao Qiu, Adam Kortylewski, Alan Yuille, Nuno Vasconcelos, and Xiaolong Wang. A-sdf: Learning disentangled signed distance functions for articulated shape representation. *arXiv preprint arXiv:2104.07645*, 2021.
- Behnam Neyshabur, Ryota Tomioka, and Nathan Srebro. In search of the real inductive bias: On the role of implicit regularization in deep learning. *arXiv preprint arXiv:1412.6614*, 2014.
- Michael Niemeyer, Lars Mescheder, Michael Oechsle, and Andreas Geiger. Differentiable volumetric rendering: Learning implicit 3d representations without 3d supervision. In *Proceedings of the IEEE/CVF Conference on Computer Vision and Pattern Recognition*, pages 3504–3515, 2020.
- Michael Oechsle, Lars Mescheder, Michael Niemeyer, Thilo Strauss, and Andreas Geiger. Texture fields: Learning texture representations in function space. In *Proceedings of the IEEE/CVF International Conference on Computer Vision*, pages 4531–4540, 2019.
- Jeong Joon Park, Peter Florence, Julian Straub, Richard Newcombe, and Steven Lovegrove. DeepSDF: Learning continuous signed distance functions for shape representation. In *Proceedings of the IEEE/CVF Conference on Computer Vision and Pattern Recognition*, pages 165–174, 2019.
- Keunhong Park, Utkarsh Sinha, Jonathan T Barron, Sofien Bouaziz, Dan B Goldman, Steven M Seitz, and Ricardo Martin-Brualla. Nerfies: Deformable neural radiance fields. In *Proceedings of the IEEE/CVF International Conference on Computer Vision*, pages 5865–5874, 2021.
- Tomaso Poggio, Qianli Liao, Brando Miranda, Andrzej Banburski, Xavier Boix, and Jack Hidary. Theory iiib: Generalization in deep networks. *arXiv preprint arXiv:1806.11379*, 2018.
- Albert Pumarola, Enric Corona, Gerard Pons-Moll, and Francesc Moreno-Noguer. D-nerf: Neural radiance fields for dynamic scenes. In *Proceedings of the IEEE/CVF Conference on Computer Vision and Pattern Recognition*, pages 10318–10327, 2021.
- Nasim Rahaman, Aristide Baratin, Devansh Arpit, Felix Draxler, Min Lin, Fred Hamprecht, Yoshua Bengio, and Aaron Courville. On the spectral bias of neural networks. In *International Conference on Machine Learning*, pages 5301–5310. PMLR, 2019.
- Sameera Ramasinghe and Simon Lucey. Beyond periodicity: Towards a unifying framework for activations in coordinate-mlps. *arXiv preprint arXiv:2111.15135*, 2021.
- Daniel Rebain, Wei Jiang, Soroosh Yazdani, Ke Li, Kwang Moo Yi, and Andrea Tagliasacchi. Derf: Decomposed radiance fields. In *Proceedings of the IEEE/CVF Conference on Computer Vision and Pattern Recognition*, pages 14153–14161, 2021.
- Daniel L Ruderman. The statistics of natural images. *Network: computation in neural systems*, 5(4): 517, 1994.

- Shunsuke Saito, Zeng Huang, Ryota Natsume, Shigeo Morishima, Angjoo Kanazawa, and Hao Li. Pifu: Pixel-aligned implicit function for high-resolution clothed human digitization. In *Proceedings of the IEEE/CVF International Conference on Computer Vision*, pages 2304–2314, 2019.
- Pedro Savarese, Itay Evron, Daniel Soudry, and Nathan Srebro. How do infinite width bounded norm networks look in function space? In *Conference on Learning Theory*, pages 2667–2690. PMLR, 2019.
- Vincent Sitzmann, Michael Zollhöfer, and Gordon Wetzstein. Scene representation networks: Continuous 3d-structure-aware neural scene representations. *arXiv preprint arXiv:1906.01618*, 2019.
- Vincent Sitzmann, Julien Martel, Alexander Bergman, David Lindell, and Gordon Wetzstein. Implicit neural representations with periodic activation functions. *Advances in Neural Information Processing Systems*, 33, 2020.
- Daniel Soudry, Elad Hoffer, Mor Shpigel Nacson, Suriya Gunasekar, and Nathan Srebro. The implicit bias of gradient descent on separable data. *The Journal of Machine Learning Research*, 19(1): 2822–2878, 2018.
- Matthew Tancik, Pratul P Srinivasan, Ben Mildenhall, Sara Fridovich-Keil, Nithin Raghavan, Utkarsh Singhal, Ravi Ramamoorthi, Jonathan T Barron, and Ren Ng. Fourier features let networks learn high frequency functions in low dimensional domains. *arXiv preprint arXiv:2006.10739*, 2020.
- Matus Telgarsky. Neural networks and rational functions. In *International Conference on Machine Learning*, pages 3387–3393. PMLR, 2017.
- Garvita Tiwari, Nikolaos Sarafianos, Tony Tung, and Gerard Pons-Moll. Neural-gif: Neural generalized implicit functions for animating people in clothing. In *Proceedings of the IEEE/CVF International Conference on Computer Vision*, pages 11708–11718, 2021.
- Grace Wahba. Smoothing noisy data with spline functions. *Numerische mathematik*, 24(5):383–393, 1975.
- Zirui Wang, Shangzhe Wu, Weidi Xie, Min Chen, and Victor Adrian Prisacariu. Nerf-: Neural radiance fields without known camera parameters. *arXiv preprint arXiv:2102.07064*, 2021.
- Fanbo Xiang, Zexiang Xu, Milos Hasan, Yannick Hold-Geoffroy, Kalyan Sunkavalli, and Hao Su. Neutex: Neural texture mapping for volumetric neural rendering. In *Proceedings of the IEEE/CVF Conference on Computer Vision and Pattern Recognition*, pages 7119–7128, 2021.
- Zhi-Qin John Xu, Yaoyu Zhang, and Yanyang Xiao. Training behavior of deep neural network in frequency domain. In *International Conference on Neural Information Processing*, pages 264–274. Springer, 2019.
- Alex Yu, Vickie Ye, Matthew Tancik, and Angjoo Kanazawa. pixelnerf: Neural radiance fields from one or few images. In *Proceedings of the IEEE/CVF Conference on Computer Vision and Pattern Recognition*, pages 4578–4587, 2021.
- Chiyuan Zhang, Samy Bengio, Moritz Hardt, Benjamin Recht, and Oriol Vinyals. Understanding deep learning requires rethinking generalization (2016). *arXiv preprint arXiv:1611.03530*, 2017.
- Chiyuan Zhang, Samy Bengio, Moritz Hardt, Benjamin Recht, and Oriol Vinyals. Understanding deep learning (still) requires rethinking generalization. *Communications of the ACM*, 64(3):107–115, 2021.
- Yaoyu Zhang, Zhi-Qin John Xu, Tao Luo, and Zheng Ma. Explicitizing an implicit bias of the frequency principle in two-layer neural networks. *arXiv preprint arXiv:1905.10264*, 2019.
- Jianqiao Zheng, Sameera Ramasinghe, and Simon Lucey. Rethinking positional encoding. *arXiv preprint arXiv:2107.02561*, 2021.

Checklist

1. For all authors...
 - (a) Do the main claims made in the abstract and introduction accurately reflect the paper's contributions and scope? [Yes]
 - (b) Did you describe the limitations of your work? [Yes]
 - (c) Did you discuss any potential negative societal impacts of your work? [N/A]
 - (d) Have you read the ethics review guidelines and ensured that your paper conforms to them? [Yes]
2. If you are including theoretical results...
 - (a) Did you state the full set of assumptions of all theoretical results? [Yes]
 - (b) Did you include complete proofs of all theoretical results? [Yes]
3. If you ran experiments...
 - (a) Did you include the code, data, and instructions needed to reproduce the main experimental results (either in the supplemental material or as a URL)? [No]
 - (b) Did you specify all the training details (e.g., data splits, hyperparameters, how they were chosen)? [Yes]
 - (c) Did you report error bars (e.g., with respect to the random seed after running experiments multiple times)? [N/A]
 - (d) Did you include the total amount of compute and the type of resources used (e.g., type of GPUs, internal cluster, or cloud provider)? [No]
4. If you are using existing assets (e.g., code, data, models) or curating/releasing new assets...
 - (a) If your work uses existing assets, did you cite the creators? [Yes]
 - (b) Did you mention the license of the assets? [N/A]
 - (c) Did you include any new assets either in the supplemental material or as a URL? [N/A]
 - (d) Did you discuss whether and how consent was obtained from people whose data you're using/curating? [N/A]
 - (e) Did you discuss whether the data you are using/curating contains personally identifiable information or offensive content? [N/A]
5. If you used crowdsourcing or conducted research with human subjects...
 - (a) Did you include the full text of instructions given to participants and screenshots, if applicable? [N/A]
 - (b) Did you describe any potential participant risks, with links to Institutional Review Board (IRB) approvals, if applicable? [N/A]
 - (c) Did you include the estimated hourly wage paid to participants and the total amount spent on participant compensation? [N/A]